Materials Advances

ROYAL SOCIETY OF CHEMISTRY

PAPER

View Article Online
View Journal | View Issue

Cite this: *Mater. Adv.*, 2025, 6, 9229

Regulated silica deposition for porosity control and mechanical enhancement of bicontinuous particle-stabilized emulsions

Meyer T. Alting and Martin F. Haase *

Bicontinuous particle-stabilized emulsions (bijels) are unique soft materials in which two immiscible liquids form an interwoven structure stabilized by colloidal particles at the interface. Their bicontinuous morphology increases the interfacial area between immiscible liquid phases, making them attractive for applications such as catalysis and energy storage. However, their mechanical fragility limits practical use. In this work, we enhance bijel robustness by depositing silica to fuse interfacial particles. We investigate a series of tetraalkoxysilanes with varying alkyl groups (methyl, ethyl, 1-propyl or 1-butyl), exhibiting decreasing reactivity. Using shorter alkyl-chain silanes and higher concentrations, we shorten the reinforcement reaction from one day to 1.5 hours. High-resolution scanning electron microscopy and small angle X-ray scattering reveal that silica deposits directionally into the aqueous domains of the bijel. Moreover, the extent of silica growth can be tailored from selectively coating interfacial particles to complete filling the aqueous channels. These findings demonstrate how the extent of silica deposition in bijels can be controlled, offering a versatile route to fabricate robust bicontinuous materials for future applications.

Received 29th August 2025,
Accepted 24th October 2025

DOI: 10.1039/d5ma00977d

rsc.li/materials-advances

1. Introduction

Bicontinuous particle-stabilized emulsions (bijels) are soft materials consisting of two interpenetrating, immiscible liquid networks stabilized by colloidal particles.[1,2] These particles strongly attach to the liquid–liquid interface, forming a jammed layer that prevents coarsening and preserves the bicontinuous morphology. This bicontinuous architecture increases the interfacial area between two immiscible phases, making bijels attractive for various applications, including biphasic catalysis,[3,4] energy storage,[5,6] filtrations[7,8] and sensors.[9] For these uses to be viable, bijels must retain their structure over time.[10] However, bijels are prone to structural destabilization, which can compromise their functionality.[3,11,12]

As-synthesized bijels are mechanically fragile and susceptible to degradation under agitation.[3,13] While individual particles attach to the interface with high energies of $\sim 10^3\ k_BT$ due to the interfacial tension, cohesion between neighboring particles is governed by weak physical forces such as van der Waals interactions.[14–16] Stronger forces, such as covalent bonds between particles, are necessary to make bijels more resilient to external forces.[10,17–19]

Van't Hoff Laboratory for Physical and Colloid Chemistry, Department of Chemistry, Debye Institute for Nanomaterials Science, Utrecht University, Utrecht, The Netherlands. E-mail: m.f.haase@uu.nl

Previous work has shown that bijels can be covalently reinforced by depositing silica on the particle scaffold. Di Vitantonio *et al.* introduced this strategy for bijels synthesized *via* solvent transfer induced phase separation (STrIPS) by adding tetraethyl orthosilicate (TEOS) to the bijel precursor mixture, where TEOS-reactions locally fuse interfacial particles.[3,20–22] Recently, Khan *et al.* demonstrated that TEOS can also be post-introduced in as-synthesized bijels, achieving similar reinforcement.[12,23,24] These studies establish the feasibility of silica deposition to reinforce bijels. However, controlling the extent and morphology of the formed silica, such as thickness, is essential for tailoring bijels into functional materials.

For instance, thin, porous silica layers are advantageous for biphasic catalysis to enhance interfacial contact between liquid phases while minimizing mass transfer limitations.[25–28] Thicker silica structures (>50 nm) can improve the mechanical stability in energy devices,[29–32] while sensor applications benefit from tunable layer thickness to tailor sensitivity and selectivity.[32–35] These examples illustrate the need to control the silica deposition in bijels.

Controlling the silica deposition using TEOS has been extensively studied for particle- and surfactant-stabilized emulsion droplets. Various parameters, such as concentration, reaction time and pH, strongly determine the extent of silica growth.[36–46] For instance, Rodriguez and Binks reported that excessive TEOS concentrations can destroy particle-stabilized

emulsion droplets due to ethanol formation, while too little can yield insufficient deposition on particle-laden interfaces.[37] Moreover, condensation of hydrolyzed TEOS at low or neutral pH is slow, which can require several days to grow sufficient silica onto the scaffold.[47,48]

These limitations of using TEOS can pose challenges to grow silica in bijels. Their interwoven liquid domain morphology differ significantly from discrete droplets, potentially resulting in different reaction kinetics and deposition pathways. Additionally, recent work showed that the liquid arrangement in bijels is transiently stable and can degrade within hours to days.[11] Although adjusting the TEOS concentration and reaction time can regulate silica deposition, the transient bijel stability calls for faster deposition to retain their bicontinuity.

A promising strategy to regulate silica deposition is by varying the alkyl chain length of the tetraalkoxysilane (TAOS). These silanes follow similar hydrolysis-condensation pathways to TEOS, but differ in reactivity.[20,49] Shorter alkyl chain silanes, like methyl, hydrolyze more rapidly due to less steric hindrance and electronic effects, accelerating silica deposition.[20,50–55] To date, various types of TAOS are already used to grow silica in particle-stabilized emulsions.[37,56–59] However, to our best knowledge, no systematic study has yet been performed on how the alkyl length affects silica deposition in bijels.

In this paper, we address this knowledge gap by systematically investigating how the alkyl chain length in TAOS regulates silica deposition and reinforcement in STrIPS-bijels. We hypothesize that more reactive, shorter alkyl-silanes accelerate silica deposition and shorten the time required to achieve mechanical robustness. To test this hypothesis, we treat bijel fibers by TAOS with varying alkyl chains: methyl, ethyl, 1-propyl or 1-butyl, corresponding to lower reactivity.[20,50–55] Using scanning electron microscopy, confocal laser scanning microscopy and small angle X-ray scattering, we show that shortening the alkyl chain from 1-propyl to methyl reduces the reinforcement time from one day to 1.5 h. We also demonstrate that increased silane concentrations can earlier disrupt the bicontinuity, and that silica grows directionally into aqueous domains. Finally, we reveal that using methyl-based silanes enables varying the silica growth from selective scaffold coating to complete filling of aqueous channels by regulating the concentration and reaction time. These results mark a step forward to advance bijels with tailored silica structures in a broad variety of applications.

2. Experimental

2.1 Materials

All chemicals were used as received. Diethyl phthalate (DEP, 99%), *n*-dodecane (99%), dodecane (mixture of isomers, density 0.7510 g mL^{-1}) glycerol (99+%, synthetic), hydrochloric acid (37%), tetrabutyl orthosilicate (TBOS, 97%) tetramethyl orthosilicate (TMOS, 99%), tetrapropyl orthosilicate (TPOS, 97%) and toluene (99+%, extra pure) were received from Thermo Scientific. Hexadecyltrimethylammonium bromide (CTAB, ≥99%), light mineral oil (density 0.84 g mL^{-1}), Nile red (for microscopy), 1-propanol (≥99.5%), sodium chloride (≥99%) and tetraethyl orthosilicate (TEOS, ≥99.0%) were purchased from Sigma-Aldrich. Silica nanoparticles (Ludox® TMA, batch no. 1003481587, diameter of 29, polydispersity <10%) were obtained from Grace GmbH. *n*-Hexane (99%, HPLC) was received from Biosolve BV. Octadecyl trichlorosilane (OTS, 94.3%) was purchased from Santa Cruz Biotechnology, Inc. Water is ultrapure MilliQ purified by a Rephile Genie U2 system (resistivity 18.2 MΩ cm).

2.2 Preparation of bijel precursor

A 34 wt% Ludox TMA dispersion is brought to pH 2.0 by adding 1 M aqueous HCl and concentrated to 45 wt% in a rotary evaporator (Heidolph Instruments) at 60 °C and 140 mbar and reacidified to pH 2.0. The dispersion is transferred to a dialysis bag (Spectra/Por MWCO 12–14 kD) and placed in a beaker containing 2.0 L MilliQ water at pH 2.0 containing 50 mM NaCl overnight. The dispersion is centrifuged at 3000 rpm for 10 minutes (Allegra X-12R, Beckman Coulter) to remove any particle aggregates and consequently diluted to 40 wt% by adding MilliQ water at pH 2.0 containing 50 mM NaCl. A bijel precursor mixture has a liquid composition (in volume fractions) of φ_{DEP} = 0.078, φ_{H_2O} = 0.435, $\varphi_{1\text{-propanol}}$ = 0.381 and $\varphi_{1\text{-glycerol}}$ = 0.106, containing 23 wt% Ludox TMA nanoparticles and 29.9 mM CTAB with the total mass/volume of the liquids, respectively. 50 mL of this precursor is prepared by mixing 3.50 mL of DEP, 6.67 mL of 200 mM CTAB in 1-propanol, 11.88 mL of a 50 wt% glycerol in 1-propanol, 2.95 mL of 1-propanol and 200 mL of the 40 wt% Ludox TMA dispersion. Additional details can be found in section MM4.2 and references.[11,23,24]

2.3 Enrichment of oils by water and glycerol

Oils were enriched by either water or both water and glycerol by vigorously mixing 80 mL of oil with 10 mL of MilliQ water at pH 2.5 or 29 wt% glycerol in MilliQ water at pH 2.5 using a magnetic stirrer for 24 hours at room temperature in a closed vial. The mixture was phase separated for at least 1 hour before using the top-layer of the oil-phase.

2.4 Glass container hydrophobization

Glass containers are treated by 3 vol% OTS in light mineral oil overnight and rinsed with *n*-hexane.

2.5 Bijel fiber extrusion

Bijels are extruded as 80 ± 10 μm width fibers using a microfluidic device consisting of coaxially aligned borosilicate glass capillaries. A round glass capillary with inner diameter (ID) 50 μm (CM Scientific, CV0508) was glued into a 300 μm ID round capillary (CV3040) and glued onto a microscopy slide using epoxy glue (Liqui Moly 6183). The inlets of both capillaries are connected through dispensing needles dispensing needles to two separate syringe pumps (World Precision Instruments, model AL-1010). The device was sequentially treated by 9 M KOH/NaOH and 3 vol% OTS solution to hydrophobized the capillary walls. The precursor mixture is injected into the

smaller capillary at a flowrate of 0.80 mL h^{-1}, and water-enriched toluene was flown through the outer capillary at 5.00 mL h^{-1}. The device was positioned vertically to a custom-made Lego® printer. The device outlet was submerged in a toluene-filled rectangular glass container (dimensions 3 cm × 5 cm) and glued onto a coverslip (4 cm × 6 cm) with Epoxy glue. Approximately 80 cm of fiber, with volume of 4.0 μL, were printed in parallel segments of 3 cm long spaced by 2 mm from each other. Additional details can be found in reference.[23]

2.6 Silica sol–gel reactions in bijels

After printing, the toluene is replaced with a 5 mL oil solution (either mineral oil, *n*-dodecane or iso-dodecane) containing dissolved TAOS in concentrations ranging between 0.01 and 3.0 vol%. For CLSM, dodecane contains Nile red. The fibers were left at room temperature for variable reaction times, depending on the experiment as discussed in the main text. For analysis by scanning electron microscopy (SEM), the oils were removed and the fibers washed several times with *n*-hexane and dried in air.

2.7 Confocal laser scanning microscopy

Bijel fibers are analyzed by inverted confocal laser scanning microscopy (CLSM, Stellaris 5, Leica Microsystems) equipped with a water-immersion objective with magnification 63×. The fibers were stored in an oil containing Nile red. Two separate excitations lasers (488 and 561 nm) are used to excite, respectively, dissolved Nile red in oil, and adsorbed Nile red on the particles. Confocal micrographs are acquired with the fluorescence emission detection ranges of, respectively, 500–550 and 600–700 nm. Additional details about CLSM analysis can be found in ref. 12 and 23.

2.8 Scanning electron microscopy analysis

The sample preparation requires evaporation of liquids in the bijels to only visualize the solid silica scaffold with the scanning electron microscope (SEM). To this end, liquids with low volatility need to be removed prior to sample drying. To remove mineral oil and dodecane, we wash the bijel samples 3 consecutive times with volatile hexane. This ''hexane only washing protocol'' has been applied for the SEM samples shown in Fig. 2, 3 and 6. To remove the polar liquid glycerol, we additionally wash 3 consecutive times with ethanol after the 3 hexane washing steps. The combined hexane/ethanol washing has been applied for the high-resolution SEM images in Fig. 7. After sample drying, bijel fibers are mounted on carbon tape supported on SEM stubs. The fibers are sputter coated with an 8 nm thick layer of platinum. The fiber's cross section and outer surface areas are imaged with scanning electron microscopy (SEM) at Phenom ProX (Thermo Fisher Scientific) and at Gemini 450 (High Resolution, Zeiss) using an acceleration voltage of 10 kV.

2.9 SAXS analysis on bijel fibers

Bijels were extruded in a synchrotron-compatible custom-made container with dimensions of 20 cm × 6 cm × 5 mm, divided into twelve separate compartments and sealed with VWR coverslips with dimensions of 6 cm × 4 cm × 0.1 mm. Each compartment is filled with 10 cm, ~80 μm width fibers extruded in toluene as described in section MM Toluene was then replaced by a 0.5 vol% TMOS in water + glycerol enriched *n*-dodecane solution for variable times between 0.25 and 7 h. Afterwards, the fibers were washed with *n*-hexane and air-dried, whereafter the container was sealed with coverslips using epoxy glue (Liqui Moly 6183).

SAXS measurements were performed at the ID02 time-resolved ultra small-angle X-ray scattering beamline at the European synchrotron radiation facility (ESRF). A 12.4 keV (wavelength λ = 0.1 mm) beam with size of 40 μm × 40 μm (FWHM) was employed. Scattering was recorded on an Eiger2 4 M detector positioned at 3 m from the sample, covering a q-range between 1.73×10^{-3} and 2.5 nm^{-1} ($q = \frac{4\pi}{\lambda}\sin\left(\frac{\theta}{2}\right)$, with θ as scattering angle). The temperature in the experimental room maintained 23.5 °C.

The bijel-filled container was vertically positioned at the beamline. For each sample, 30 frames with an exposure time of 0.10 s per frame were collected. An empty compartment was measured for reference and background subtraction procedures. Scattering patterns were normalized to absolute intensity and reduced to 1D patterns according to standard procedures.[60] 1D patterns were averaged using all frames acquired per measurement and background-corrected using SAXSutilities2 software.[61] Further analysis was done by OriginPro software. Unless stated otherwise, all 1D scattering profiles and analyzed data shown in this chapter are background corrected.

2.10 N_2 physisorption

N_2 adsorption–desorption isotherms were recorded at −196 °C using a Micromeritics TriStar II Plus apparatus, following standard IUPAC procedures.[62,63] Approximately 0.05 g of TEOS-treated bijel fibers has been used. Prior to analysis, fibers were washed with ethanol, 1-propanol, air-dried and outgassed under vacuum at 60 °C for 72 h. The specific surface area was determined using Brunauer–Emmett–Teller (BET) analysis, and average pore size is calculated using the Barrett–Joyner–Halenda (BJH) method.

For sample preparation, 2 mL of bijel fiber were extruded using a rotating water-enriched toluene reservoir (see ref. 8) with a total volume of 150 mL. The fibers were subsequently treated with 3 vol% TEOS in mineral oil for 24 h. After the TEOS treatment, the fibers were washed with ethanol, 1-propanol and *n*-hexane, then air-dried at 110 °C. Notably, the addition of ethanol and 1-propanol caused as-synthesized fibers to redisperse, resulting in loss of the bijel structure. Therefore, only TEOS-treated fibers were analyzed to assess the porosity of the deposited silica layer.

3. Results and discussion

3.1 Bijel reinforcement using tetraalkoxysilane reactions

In this study, bijels are fabricated as fibers with diameters of 80 ± 10 μm *via* STrIPS.[64,65] The fibers are stored in a glass

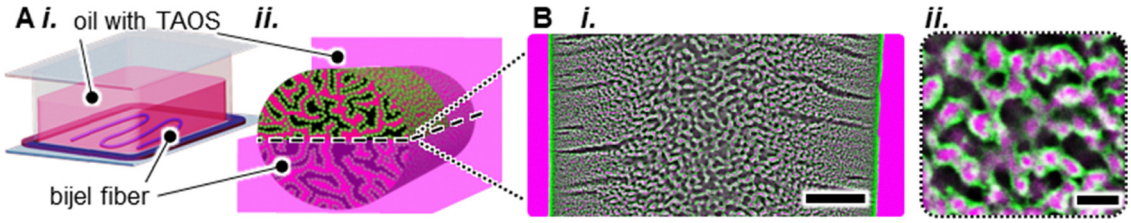

Fig. 1 Experimental system. (A) Experimental setup of (i) glass container filled with oil containing TAOS and bijel fiber. (ii) 3D schematics of bijel fiber in oil on how TAOS diffuses into the oil-network of a bijel. (B) (i) CLSM image of equator of bijel fiber segment stored in *n*-hexane with oil (magenta), aqueous (black) and particle-network (green) processed with a bandpass filter. Scale bar = 20 μm. (ii) Magnified confocal image of oil- and aqueous pores, scale bar = 3 μm.

container filled with 10 mL water-enriched oil (either mineral oil or dodecane) containing dissolved TAOS, as schematically depicted in Fig. 1(A)-i.

The bijel fibers used in this study are stabilized by 29 nm Ludox TMA silica nanoparticles functionalized by cetyltrimethylammonium bromide (CTAB). Fig. 1(A)-ii schematically shows a cylindrical bijel fiber and marks the equatorial plane. Fig. 1(B)-i shows a confocal laser scanning microscopy (CLSM) image of the equatorial cross-section, which is magnified in Fig. 1(B)-ii. This image reveals the interconnected oil (magenta) and aqueous (black) networks, separated by nanoparticles (green). The interwoven networks exhibit an increasing pore size gradient towards the center of the fiber, containing large aqueous macrovoids that extend radially inward. At the fiber's outer surface, pores are present that connects the oil network with the surrounding oil.[24] These structural characteristics arise from diffusion phenomena during STrIPS.[12,23,24] The aqueous phase in these bijels consists of water and glycerol. The addition of glycerol is needed to reduce light scattering to enable confocal microscopy imaging of these bijels.[23] In this chapter, we will vary the type of TAOS to investigate silica deposition on the CTAB-functionalized particle scaffold.

After fiber fabrication *via* STrIPS, the surrounding oil is exchanged with a mineral oil solution containing TAOS. TAOS diffuses into the fiber where water initiates hydrolysis. The hydrolyzed species can condense onto silica particles, fusing them to reinforce the scaffold. Notably, as TAOS hydrolysis typically yields partially hydrolyzed silanes, the deposited material contains residual alkoxy groups.[22,66,67] We refer to this deposited material as 'hybrid silica'. The extent of reinforcement depends on the amount of hybrid silica deposited, which is governed by the reactivity of the TAOS precursor.

We hypothesize that less reactive TAOS precursors deposit insufficient hybrid silica to reinforce the particle scaffold. To study this reactivity effect, we compare four TAOS molecules with increasing alkyl chain lengths: tetramethyl- (TMOS), tetraethyl- (TEOS), tetrapropyl (TPOS) and tetrabutyl orthosilicate (TBOS) as shown in Fig. 2(A). Their hydrolysis rates decrease in the order TMOS > TEOS > TPOS > TBOS.[54,55]

To test our hypothesis, we treat bijel fibers with 3 vol% of each TAOS precursor in water-enriched mineral oil for 24 h. Afterwards, fibers are washed with *n*-hexane and air-dried. We employ scanning electron microscopy (SEM) to assess the structural reinforcement of fibers. Since SEM requires drying of the fibers, the scaffold can collapse (see S1). Depositing hybrid silica in bijels can stabilize the scaffold to prevent collapse. The extent to which the bijel structure is retained after drying provides a qualitative measure of the reinforcement by each TAOS precursor.

Fig. 2(B) shows SEM images of fiber cross-sections after TAOS treatment. Three main observations can be made for the different four different TAOS reactants: (I) TMOS leads to partial filling of the void spaces with hybrid silica, (II) the void spaces remain empty after TEOS- and TPOS-treatment while retaining the scaffold, and (III) the scaffold is collapsed for the TBOS-treated fibers.

These three findings support the reactivity hypothesis depicted in Fig. 2(A). TMOS has the shortest alkyl moieties, therefore the highest reactivity, resulting in the uncontrolled deposition of hybrid silica. TEOS and TPOS have intermediate alkyl lengths, facilitating moderated reactivity and hence regulated silica deposition. Last, TBOS with the longest alkyl moieties is the least reactive, resulting in insufficient hybrid silica deposition to stabilize the scaffold. In the following, we first focus on hybrid silica deposition with TEOS and TPOS, since Fig. 2(B) shows that both enable the stabilization of the bijel structure after drying without excessive hybrid silica deposition. We first ask how their concentrations and treatment times affect bijel stabilization.

To answer this question, we treat bijel fibers with 3, 0.3 or 0.03 vol% of TEOS or TPOS in water-enriched mineral oil for reaction times ranging between 7 and 72 h. Fig. 3 shows SEM images of the dried bijel fibers for 3 and 0.3 vol% (0.03 vol% is excluded, since they show similar structures as for 0.3 vol%, see S2). We draw also here three main observations about the scaffold stabilization: (I) both TEOS and TPOS require 3 vol% to obtain the desired stabilization, whereas 0.3 vol% leads to collapsed structures for reaction times < 72 hours, (II) TEOS achieves stabilization from 7 h on, while TPOS requires 24 h, (III) for 3 vol% TEOS, void spaces become partially filled with hybrid silica after 72 h.

While a minimum TAOS concentration is needed to stabilize the scaffold, observations (II) and (III) are also in agreement with the reactivity hypothesis. The higher reactivity of TEOS allows for faster stabilization of the scaffold compared to TPOS. Also, the partial filling of the void spaces during TEOS reaction after 72 h reflects the higher reactivity than for TPOS.

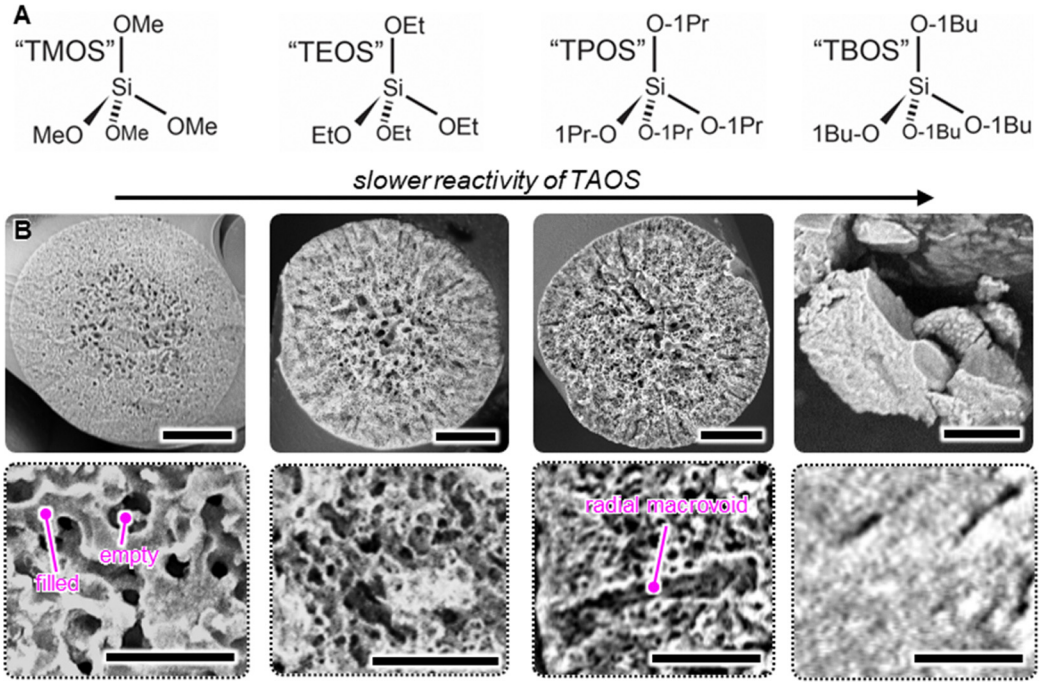

Fig. 2 Effect of alkyl chain length of TAOS on reinforcement of bijel structure. (A) Structure of TMOS, TEOS, TPOS and TBOS sorted by slower reactivity. (B) SEM images of bijel structure after 24 h reaction with 3 vol% TAOS in water-enriched mineral oil, washed with *n*-hexane and air-dried, where some glycerol could remain in the bijel network. Insets for TEOS and TPOS-treated fibers indicate different pore morphologies in bijels: voids refer to the interconnected void spaces in the structure, whereas a radial macrovoid is a large, channel-like feature extending from the outer surface inward and surrounded by interwoven void spaces. Scale bar = 20 μm in large image, 3 μm in inset.

The partial filling of void spaces with TMOS (Fig. 2(B)) and TEOS (Fig. 3(A), 72 h) demonstrates that hybrid silica deposition within the bijel can be spatially controlled. In contrast, void filling was not observed with TPOS under the conditions tested, although longer reaction times may enable it. Additional evidence of void filling with TMOS, and its implications for porosity control, are presented in Sections 3.3 and 3.4.

SEM analysis provides direct information on the stabilization of the scaffold after drying. But, SEM analysis does not reveal what happens during the TAOS treatments when stored in the continuous oil phase. An important criterium for bijel stability is also whether the arrangement of the liquid networks remains intact, as studied in the next section.

3.2 Dynamics of tetraalkoxysilane bijel treatment

To observe the liquid arrangement during TAOS treatment, we employ confocal laser scanning microscopy (CLSM). To this end, the mineral oil is replaced by dodecane to reduce the refractive index mismatch between the bijel and the surrounding oil, thereby reducing light scattering for enabling CLSM. We compare bijel stability during TEOS reaction using 3 and 0.3 vol%. The magnified CLSM images of Fig. 4(A)-i show that for 3 vol% TEOS after 4 h, magenta-colored oil penetrates into the black-colored aqueous phase. During this process, the green-labeled particle scaffold remains intact. Also, for 0.3 vol% TEOS, oil partially displaces the aqueous phase after 1.5 h as shown in Fig. 4(A)-ii. However, for 0.3 vol% TEOS, the particle scaffold moves together with the liquid–liquid interface. Thus, liquid rearrangements occur during TEOS reaction, but the rigidification of the particle scaffold requires a minimum TEOS concentration.

Interestingly, the onset time of the liquid destabilization is faster for TEOS compared to TPOS. Fig. 4(B) plots the stability time of bijels during TAOS treatment plotted against TAOS concentration. We define the stability time of a bijel as the point at which oil displacement into the bijel is first visibly apparent in CLSM images (see S4). For TEOS, the stability time increases from 50 min at 3 vol% to 210 min for 0.03 vol% and below. A similar trend is observed for TPOS, where the stability time enhances from 80 min to 210 min over the same concentration range. In the absence of TAOS, bijels also remain stable for 210 min, consistent with the transient stability of STrIPS-bijels when stored in oil as previously studied.[11] These results suggest that at concentrations of 0.3 vol% and above, both TEOS and TPOS treatments significantly reduce bijel stability. Apparently, the TAOS reaction triggers destabilization of the liquid network, with the more reactive TEOS inducing faster destabilization.

To better understand this destabilization mechanism, we quantify the change in fiber diameter over time. Recent studies have shown that STrIPS-bijels stored in oil can gradually lose their aqueous phase, which leads to a shrinkage of the fiber volume and correspondingly, decrease in fiber diameter.[11] Fig. 5(A) and (B) show CLSM time series of the equatorial plane of bijel fibers during treatment with 0.3 vol% TPOS and TEOS, respectively. Both CLSM series show that the fiber diameter

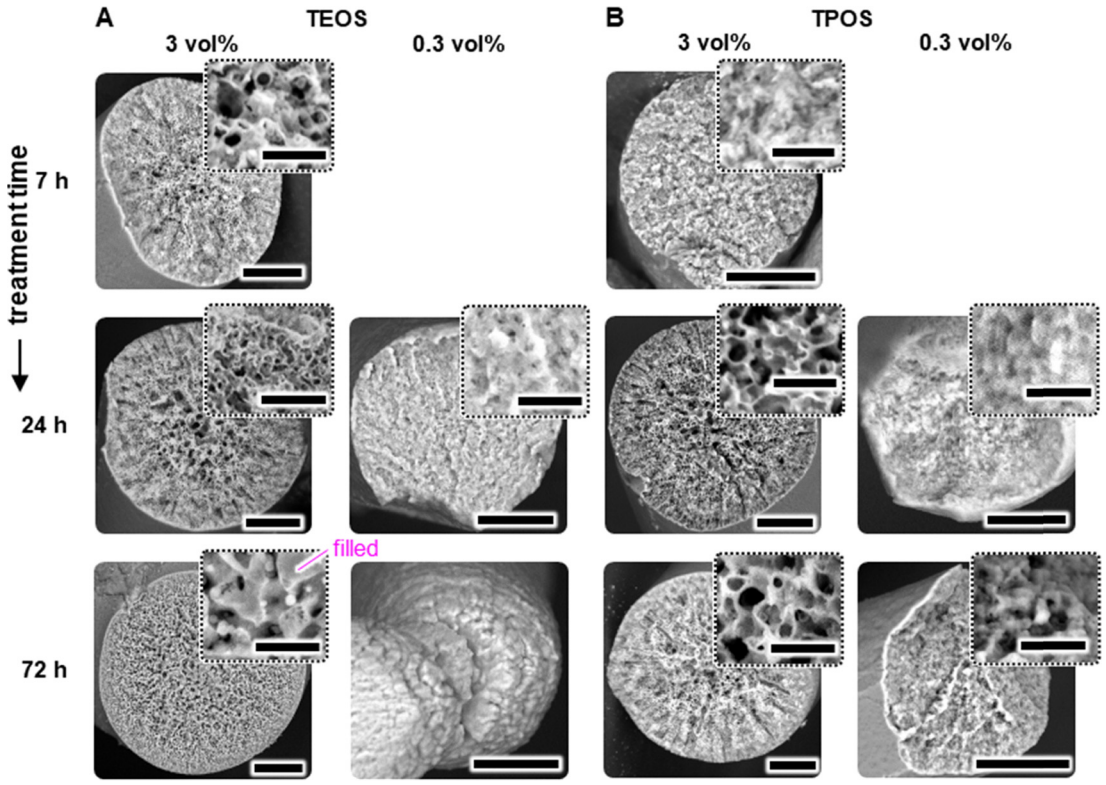

Fig. 3 Effect of TAOS concentration and treatment time. SEM images of dried bijel fibers treated with variable (A) TEOS, and (B) TPOS concentrations and reaction times. Fibers are washed with *n*-hexane, which can leave some glycerol in the bijel network. Scale bars are 20 μm, within insets are 5 μm.

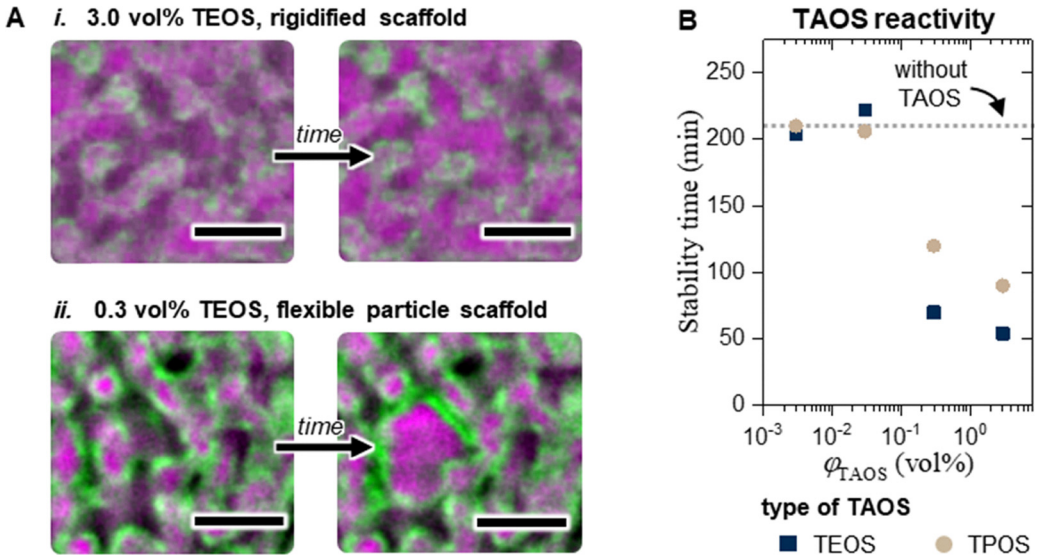

Fig. 4 Bijel stability during TAOS treatment. (A) Magnified CLSM time images of bijel network near fiber center during treatment with (i) 3.0 after 4 h and (ii) 0.3 vol% and 1.5 h TEOS in water-enriched iso-dodecane. Time step between images is 4 min. Scale bars in CLSM images are 4 μm. (B) Stability time of bijels as function of TAOS concentration in water-enriched iso-dodecane.

decreases during both treatments, compacting the bicontinuous network. We quantify this decrease in fiber diameter by estimating the fiber volume at time t, $V(t)$, assuming a cylindrical geometry, and normalize it by initial fiber volume V_0, yielding the ratio V/V_0.

Interestingly, V/V_0 decreases faster for TEOS compared to TPOS. Fig. 5(C) plots V/V_0 over time during 0.3 vol% TEOS and TPOS-treatments, and in absence of TAOS. With TEOS, V/V_0 continuously decreases from $t = 0$ min on, while with TPOS, the fiber volume remains constant for ~70 min before a similar

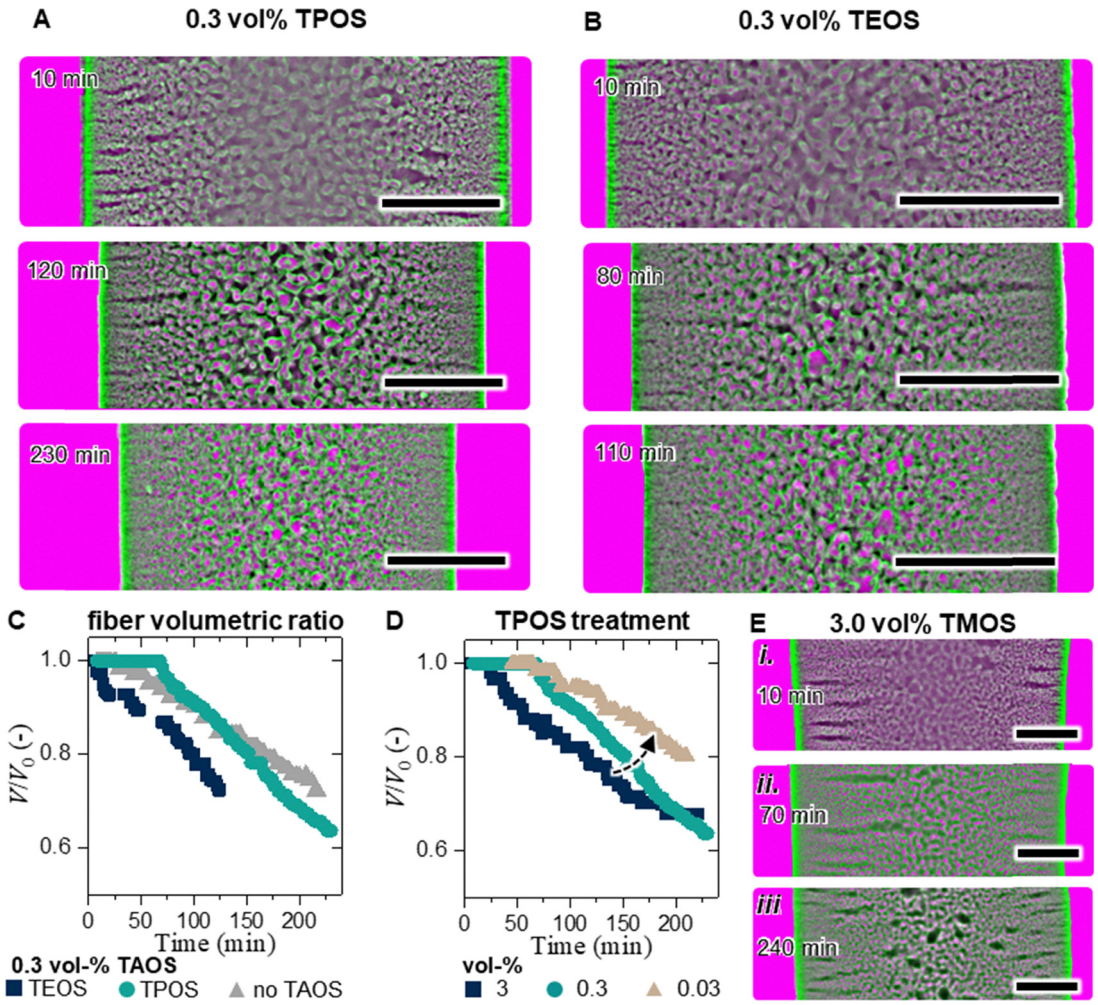

Fig. 5 Bijel destabilization during TAOS treatment. (A) + (B) CLSM time series of bijel fiber during treatment with (A) 0.3 vol% TPOS, (B) 0.3 vol% TEOS in water-enriched iso-dodecane. Scale bar is 20 μm. (C) Normalized volumetric change of bijel fiber V/V_0 over time during 0.3 vol% TAOS treatment in water-enriched iso-dodecane. (D) V/V_0 against time for bijel fiber during TPOS treatment in water-enriched iso-dodecane. (E) CLSM time series of bijel during a 3 vol% TMOS treatment in water + glycerol enriched *n*-dodecane. Scale bar is 20 μm.

decline in V/V_0 is observed. In the absence of TAOS, V/V_0 also begins to decrease from t = 25 min on with a similar trend as observed with TPOS.

For a given type of TAOS, raising the concentration increases the rate of the V/V_0 reduction. Fig. 5(D) plots V/V_0 over time for bijel fibers treated with TPOS for varying concentrations (data for TEOS in S3). For 3 vol% TPOS, V/V_0 decreases from 25 min on, while for 0.3 and 0.03 vol%, the onset of fiber shrinkage is extended to 75 min. Moreover, V/V_0 decreases more rapidly for 0.3 vol% than for 0.03 vol% TPOS. Thus, higher TAOS concentration accelerates the destabilization of the liquid re-arrangement in bijels.

What causes the TAOS reaction to destabilize the liquid networks? Previous work on STrIPS-bijels has shown that the aqueous phase can dissolve in the surrounding oil in absence of TAOS. During TAOS treatment, this destabilization accelerates with increasing TAOS reactivity and concentration. Possible explanations are as follows: (i) the more reactive TAOS produces alcohol at a faster rate, potentially promoting faster dissolution of water from the bijel into the surrounding oil. However, this effect is limited by the lower solubility of water in oil associated with the type of alcohol generated by the more reactive TAOS reagent. The solubility of water in oil decreases as the alcohol type changes from 1-propanol to ethanol to methanol (see S11). (ii) Another possible explanation for the faster bijel destabilization observed with increasing TAOS reactivity and concentration is that the deposited hybrid silica is inherently hydrophobic, thereby rendering the scaffold more hydrophobic (see S5). This hydrophobization can cause water to dewet the surface so that the aqueous phase flows out of the bijel. Both mechanisms could explain the accelerated loss of the aqueous phase during TAOS treatment. However, further research is needed to identify the exact destabilization mechanisms.

Is it possible to preserve the liquid arrangement of the bijel structure during TAOS treatment? To address this question, we perform CLSM analysis on bijels during a TMOS reaction. Fig. 5(E) shows a CLSM time series of a bijel fiber treated with 3 vol% TMOS. Over 240 minutes, three observations can be

made: (I) the image contrast of the fiber interior improves, (II) the initially black-labeled aqueous domains become fluorescent around 70 min and reappear black within 240 min, and (III) the fiber diameter remains unchanged.

The transient fluorescence of the aqueous network likely arises from methanol formation during TMOS hydrolysis. Methanol can partition into the aqueous phase, which can withdraw fluorescent Nile red from the oil phase (see S6). Due to the poor solubility of Nile red in water, this emission diminishes over time (see S6).[68]

These three observations suggest that the liquid networks are preserved during TMOS treatment, in contrast to the destabilization observed with TEOS and TPOS (see S7). However, SEM analysis of TMOS treated fibers in Fig. 2(B) shows that TMOS also leads to excessive deposition of hybrid silica, filling the void spaces in the structure. CLSM cannot resolve whether such silica overgrowth occurs. In the following section, we investigate whether the TMOS reaction conditions can be adjusted to reinforce the bijel scaffold while keeping the void spaces open.

3.3 Controlling hybrid silica deposition in TMOS-treated Bijels

To investigate the deposition of hybrid silica from TMOS, we treat bijel fibers with varying TMOS concentrations and treatment times and analyze the structures using SEM. Bijels are treated in water + glycerol enriched *n*-dodecane and sequentially washed and air-dried. Fig. 6(A) shows SEM images of bijels treated for 7 h with TMOS concentrations ranging from 0.01 to 1.00 vol%. From these images, three types of bijel

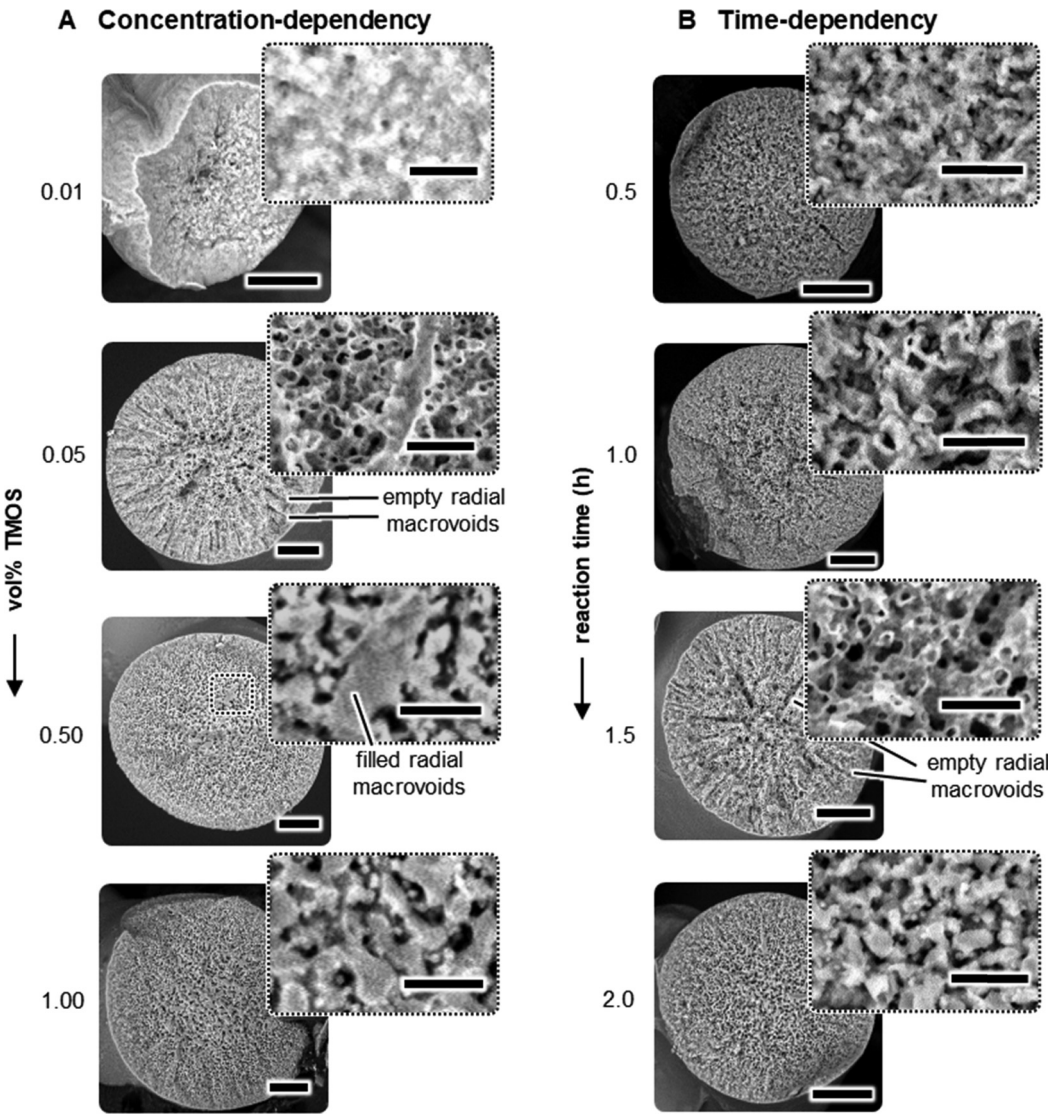

Fig. 6 Stability of bijel scaffold after TMOS treatment. SEM images of dried bijel fibers after TMOS treatment by (A) various concentrations after 7 h reaction, and (B) longer treatment times using 0.5 vol% TMOS. Fibers are washed with (A) *n*-hexane and (B) ethanol. Washing with *n*-hexane can leave some glycerol in (A), whereas ethanol removes all glycerol in (B). The presence of radial macrovoids in fibers exhibiting a retained structure with only empty void spaces are indicated. Scale bars are 20 μm, in insets are 4 μm.

structures can be observed: (I) at low TMOS concentrations of 0.01 vol%, the scaffold collapses, (II) at intermediate concentrations of 0.05 and 0.10 vol%, the scaffold retains with empty void spaces and observable radial macrovoids, and (III) for higher concentrations from 0.50 vol% on, part of the void spaces are filled with hybrid silica, and radial macrovoids are filled or disappeared.

A similar trend is observed when varying the treatment time at a fixed TMOS concentration of 0.50 vol% as shown in Fig. 6(B): (I) short durations of 1 h and less lead to collapsed structures, (II) at 1.5 h, the scaffold is retained with open void spaces, and (III) longer durations from 2 h on result in partially filled void spaces and vanished radial macrovoids.

These results show that both TMOS concentration and treatment time affect the rate of hybrid silica deposition in the same way. Higher concentrations allow for shorter treatment times to reinforce the scaffold while maintaining empty voids spaces. Beyond a certain threshold concentration or treatment time, excessive silica deposition can occur. Thus, varying either the concentration or treatment time of the TMOS reaction allows to regulate the extend of silica deposition in bijels.

The partial filling of void spaces during TMOS treatment, where some void spaces become completely filled with hybrid silica while leaving other ones empty, raises the question: does hybrid silica grow towards the aqueous or oil channels in the bijel? In the following, we explore how hybrid silica deposits in bijels when using TMOS by combining small angle X-ray scattering (SAXS) with high-resolution SEM (HR-SEM).

3.4 Growth direction of hybrid silica in TMOS-treated Bijels

We employ SAXS on dried bijel fibers to study how hybrid silica deposition alters the morphology of the particle scaffold. SAXS probes structural features such as particle shape, and can reveal morphological changes during TMOS treatment.[69,70] In the data presented here, the scattering vector q ranges from 0.1 to 1.0 nm^{-1}, corresponding to real-space distances from ~60 to ~6 nm, to probe structural features on the nanoparticle scale.

Fig. 7(A)-i plots the scattering intensity profiles, $I(q)$, against q for bijels treated with 0.5 vol% TMOS for durations between 0.25 and 7 h. At 0.25 h, fringes are observed for $q > 0.2$ nm^{-1}, which are characteristic for individual spherical nanoparticles such as Ludox TMA. These fringes become less pronounced with longer treatments up to 1.5 h. This change in $I(q)$ is highlighted in Fig. 7(A)-ii, which magnifies the flattening of a minimum near q = 0.34 nm^{-1}. Beyond 1.5 h, $I(q)$ remains unchanged within this q-range.

The gradual flattening of the fringes indicates that the initially spherical particle shape become less defined over time. This suggests that hybrid silica deposits onto the particle scaffold that can reinforce the structure. This interpretation is consistent with SEM images in Fig. 7(B), which shows a reinforced scaffold after 1.5 h treatment with open void spaces.

Beyond 1.5 h of TMOS treatment, SEM reveals that part of the void spaces are filled with hybrid silica, while SAXS shows no further structural development. This discrepancy suggests that hybrid silica deposits on length scales above 100 nm, which are inaccessible by SAXS. To examine these

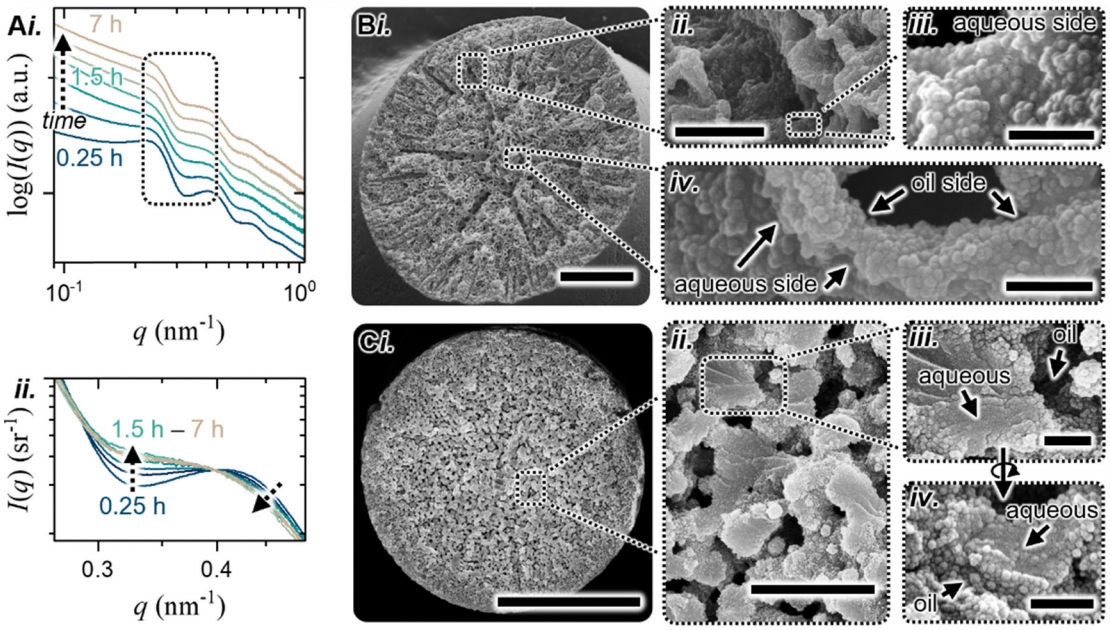

Fig. 7 Mechanistic insights of hybrid silica deposition out of TMOS in bijels. (A) SAXS analysis of bijel fibers of measured scattering intensity $I(q)$ against scattering vector q for (i) entire q-range (stacked with a y-offset of 0.3), and (ii) q-region between 0.3 and 0.4 nm^{-1}. (B) + (C) Magnified HR-SEM of fiber cross sections treated with 0.5 vol% TMOS after (B) 1.5 h and (C) 7 h with magnification of particle scaffold exposed to oil- and aqueous phase. Fibers are washed with n-hexane and ethanol, which probably removed all glycerol from the structure. Scale bars are: (i) 20 μm, (ii) 2 μm, (iii + iv): 300 nm.

larger structures, we use high-resolution SEM (HR-SEM) to visualize the scaffold of bijel fibers treated by 0.5 vol% TMOS with empty-only or partially filled voids.

Fig. 7(B)-i shows an HR-SEM image of a fiber cross-section after 1.5 h reaction, featuring a preserved scaffold with empty voids. Magnified images of a radial macrovoid in Fig. 7(B)-ii and iii reveal that scaffold particles are embedded in hybrid silica and appear less spherical. In contrast, a scaffold exposed to two distinct pores in Fig. 7(B)-iv shows that one side (facing downward) is covered by hybrid silica, while the other side (facing upward) is uncoated. Also, particles located on the outer fiber surface, exposed to the continuous oil phase, remain uncoated (see S8).

After 7 h of TMOS treatment, both filled and empty voids are observed in the cross-section in Fig. 7(C)-i and ii. In filled regions in Fig. 7(C)-iii, particles are embedded in silica, whereas particles bordering empty voids remain uncoated as seen in Fig. 7(C)-iv.

These observations suggest that hybrid silica grows directionally toward one liquid phase rather than depositing uniformly around the scaffold. The embedded particles in the radial macrovoid in Fig. 7(B)-iii were initially exposed to the aqueous phase, while uncoated particles in Fig. 7(B)-iv faced the oil phase containing TMOS (see S8). Additionally, the filled radial macrovoid in Fig. 6(A) (0.5 vol% TMOS) indicates that this initially aqueous-filled domain becomes completely loaded with hybrid silica. We conclude that hybrid silica during TMOS treatment preferentially grows towards the aqueous phase in bijels. This conclusion is supported by previous studies on TMOS-based silica growth in water-in-oil particle-stabilized emulsions, which showed that silica formed from TMOS preferentially grow towards the water phase.[37,71,72]

Following the directional silica growth, we note that radial macrovoids are no longer observed in SEM images of TMOS-treated fibers with silica-filled aqueous channels in Fig. 6 and 7. However, these macrovoids are visible in CLSM during TMOS treatment in Fig. 5(E) and in SEM when aqueous channels remain unfilled (Fig. 7(B)). In this work, we are not able to clarify these observations. However, within our ongoing work, we aim at providing additional data to understand the effect of TMOS treatment on the radial macrovoids.

Before concluding, we discuss the mechanical properties of bijel fibers after various TAOS treatments. TAOS deposition not only prevents the bijel morphology from collapsing during drying, but also significantly enhances the bending and tensile strength of the fibers (see S1 and S9). While untreated fibers are mechanically fragile and prone to collapse upon drying, fibers treated with TMOS, TEOS or TPOS retain their morphology and can be transferred or integrated into devices without structural degradation,[12] though they remain brittle. In contrast, fibers with silica-filled aqueous voids exhibit enhanced flexibility, withstanding bending without breaking. These findings show that hybrid silica growth not only reinforces bijels, but also allows tuning of the mechanical performance from brittle to flexible by regulating the extent of hybrid silica deposition.

The ability to regulate the extent of silica deposition paves the way for advancing bijels towards various applications. Bijel with retained scaffolds and open channels are well-suited in *e.g.* biphasic catalysis and liquid–liquid extraction, where interfacial contact and mass transfer between immiscible liquids are essential.[12,73] BET analysis confirms that the hybrid silica layer is porous (see S10). In contrast, structures with silica-filled filled aqueous networks and open oil channels offer opportunities in energy storage,[74–76] by immobilizing charge-storing materials within a continuous matrix, and as template material for robust separation membranes.[7,8,77] Finally, tuning the silica thickness enables the design of porous coatings for sensor applications, where layer thickness regulate sensitivity.[32–35] Together, these examples illustrate how controlled silica deposition can transform these bicontinuous structures into mechanically robust and functional, versatile materials.

4. Conclusions

This study demonstrates how silica deposition in STrIPS-bijels can be regulated to reinforce the particle scaffold, offering a versatile route to fabricate robust structures with broad application potential. While previous studies established the feasibility of covalently reinforcing bijels *via* silica deposition, this work provides results on how the extent of deposition can be tailored. The bijels studied consist of two interpenetrating liquid networks, stabilized by an interfacial layer of CTAB-functionalized silica nanoparticles. We explore how treating these bijels with tetraalkoxysilanes (TAOS) with varying alkyl chain lengths (methyl, ethyl, 1-propyl or 1-butyl) affects silica deposition. We reveal that silica deposition occurs directionally towards the aqueous domains and is governed by: (I) alkyl chain length, where shorter chains accelerates deposition, reducing the treatment time to achieve reinforcement from one day to 1.5 h, and (II) silane concentration and treatment time, which both tailor the extent of deposition from selectively coating the interfacial scaffold to complete filling of the aqueous channels. Additionally, we observe that the reinforcement reaction can affect the bicontinuous liquid architecture, depending on the silane concentration. Moreover, we demonstrate, for the first time, that the extent of silica deposition can be tailored from selective scaffold coating to complete filling of the aqueous channels using methyl-based TAOS by adjusting the silane concentration and reaction time. The ability to regulate silica deposition in bijels open up new strategies for developing robust, functional bijel materials in fields like catalysis, separations, sensing and energy storage.

Author contributions

Meyer T. Alting: conceptualization, methodology, investigation, visualization, data curation, writing – original draft. Martin F. Haase: conceptualization, methodology, writing – original draft, Supervision, project administration, funding acquisition.

Conflicts of interest

The authors declare no competing financial interest.

Data availability

The data supporting this article have been included as part of the supplementary information (SI). Supplementary information is available. See DOI: https://doi.org/10.1039/d5ma00977d.

Acknowledgements

This project has received funding from the European Research Council (ERC) under the European Union's Horizon 2020 research and innovation program (grant agreement no. 802636). The authors thank Dominique Thies-Weesie and Mariska de Ruiter for performing HR-SEM imaging and Remco Dalebout for N_2-physisorption measurements. The authors are grateful for the European Synchrotron Radiation Facility, in particular the technical team of the ID02 beamline for supporting SAXS experiments (proposal SC-5514). During the preparation of this paper, the authors used Chat GPT-4o to improve the sentence structure and grammar of the Abstract, last paragraph of the introduction, first paragraphs of Section 3.2, last paragraph of Section 3.4, Conclusion and S6. After using this tool, the authors reviewed and edited the content as needed and take full responsibility for the content of this chapter.

References

1 M. E. Cates and P. S. Clegg, Bijels: A New Class of Soft Materials, *Soft Matter*, 2008, **4**(11), 2132–2138, DOI: 10.1039/b807312k.
2 K. Stratford, R. Adhikari, I. Pagonabarraga, J. C. Desplat and M. E. Cates, Colloidal Jamming at Interfaces: A Route to Fluid-Bicontinuous Gels, *Science*, 2005, **309**(5744), 2198–2201, DOI: 10.1126/science.1116589.
3 G. Di Vitantonio, T. Wang, M. F. Haase, K. J. Stebe and D. Lee, Robust Bijels for Reactive Separation *via* Silica-Reinforced Nanoparticle Layers, *ACS Nano*, 2019, **13**, 26–31, DOI: 10.1021/acsnano.8b05718.
4 T. Park, G. H. Choi, D. Lee and P. J. Yoo, Metal-Phenolic Network-Coated Hollow Fiber Catalytic Membranes *via* Solvent Transfer Induced Phase Separation (STRIPS) for Suzuki Coupling Reaction, *J. Membr. Sci.*, 2021, **634**, 119386, DOI: 10.1016/j.memsci.2021.119386.
5 D. Cai, F. H. Richter, J. H. J. Thijssen, P. G. Bruce and P. S. Clegg, Direct Transformation of Bijels into Bicontinuous Composite Electrolytes Using a Pre-Mix Containing Lithium Salt, *Mater. Horiz.*, 2018, **5**, 499–505, DOI: 10.1039/c7mh01038a.
6 J. A. Witt, D. R. Mumm and A. Mohraz, Microstructural Tunability of Co-Continuous Bijel-Derived Electrodes to Provide High Energy and Power Densities, *J. Mater. Chem. A*, 2016, **4**(3), 1000–1007, DOI: 10.1039/c5ta06260h.
7 M. F. Haase, H. Jeon, N. Hough, J. H. Kim, K. J. Stebe and D. Lee, Multifunctional Nanocomposite Hollow Fiber Membranes by Solvent Transfer Induced Phase Separation, *Nat. Commun.*, 2017, **8**, 1234, DOI: 10.1038/s41467-017-01409-3.
8 H. Siegel, A. J. Sprockel, M. S. Schwenger, J. M. Steenhoff, I. Achterhuis, W. M. De Vos and M. F. Haase, Synthesis and Polyelectrolyte Functionalization of Hollow Fiber Membranes Formed by Solvent Transfer Induced Phase Separation, *ACS Appl. Mater. Interfaces*, 2022, **14**(38), 43195–43206, DOI: 10.1021/acsami.2c10343.
9 M. N. Lee and A. Mohraz, Bicontinuous Macroporous Materials from Bijel Templates, *Adv. Mater.*, 2010, **22**(43), 4836–4841, DOI: 10.1002/adma.201001696.
10 M. Zhang, L. Wei, H. Chen, Z. Du, B. P. Binks and H. Yang, Compartmentalized Droplets for Continuous Flow Liquid-Liquid Interface Catalysis, *J. Am. Chem. Soc.*, 2016, **138**, 10173–10183, DOI: 10.1021/jacs.6b04265.
11 M. T. Alting and M. F. Haase, Stabilizing Bicontinuous Particle-Stabilized Emulsions Formed *via* Solvent Transfer-Induced Phase Separation, *Soft Matter*, 2025, **21**, 760–769, DOI: 10.1039/d4sm01213e.
12 M. A. Khan, A. J. Sprockel, K. A. Macmillan, M. T. Alting, S. P. Kharal, S. Boakye-Ansah and M. F. Haase, Nanostructured, Fluid-Bicontinuous Gels for Continuous-Flow Liquid–Liquid Extraction, *Adv. Mater.*, 2022, **34**, 2109547, DOI: 10.1002/adma.202109547.
13 V. Poulichet and V. Garbin, Ultrafast Desorption of Colloidal Particles from Fluid Interfaces, *Proc. Natl. Acad. Sci. U. S. A.*, 2015, **112**(19), 5932–5937, DOI: 10.1073/pnas.1504776112.
14 B. P. Binks and T. S. Horozov, *Colloidal Particles at Liquid Interfaces*, 2006.
15 M. N. Lee, J. H. J. Thijssen, J. A. Witt, P. S. Clegg and A. Mohraz, Making a Robust Interfacial Scaffold: Bijel Rheology and Its Link to Processability, *Adv. Funct. Mater.*, 2013, **23**(4), 417–423, DOI: 10.1002/adfm.201201090.
16 S. Levine, B. D. Bowen and S. J. Partridge, Stabilization of Emulsions by Fine Particles I. Partitioning of Particles between Continuous Phase and Oil/Water Interface, *Colloids Surf.*, 1989, **38**(2), 325–343, DOI: 10.1016/0166-6622(89)80271-9.
17 P. J. Baricelli, J. C. Pereira and M. Rosales, Aqueous-Biphasic Catalysis: A Technological Alternative for the Use of Organometallic Complexes in Hydrogenation and Hydroformylation Reactions with Possible Industrial Application, *Catal. Today*, 2025, **443**, 114969, DOI: 10.1016/j.cattod.2024.114969.
18 M. Schrimpf, P. A. Graefe, A. Holl, A. J. Vorholt and W. Leitner, Effect of Liquid-Liquid Interfacial Area on Biphasic Catalysis Exemplified by Hydroformylation, *ACS Catal.*, 2022, **12**(13), 7850–7861, DOI: 10.1021/acscatal.2c01972.
19 F. Jutz, J. M. Andanson and A. Baiker, Ionic Liquids and Dense Carbon Dioxide: A Beneficial Biphasic System for Catalysis, *Chem. Rev.*, 2011, **111**(2), 322–353, DOI: 10.1021/cr100194q.
20 T. N. M. Bernards, M. J. van Bommel and A. H. Boonstra, Hydrolysis-Condensation Processes of the Tetra-Alkoxysilanes

TPOS, TEOS and TMOS in Some Alcoholic Solvents, *J. Non-Cryst. Solids*, 1991, **134**(1–2), 1–13, DOI: 10.1016/0022-3093(91)90005-Q.

21 C. J. Brinker, Hydrolysis and Condensation of Silicates: Effects on Structure, *J. Non-Cryst. Solids*, 1988, **100**, 31–50.

22 C. J. Brinker, D. W. Schaefer, B. D. Assink, B. D. Kay, K. D. Keefer and C. S. Ashley, Sol–Gel Transition in Simple Silicates II – Basic Investigations on Hydrolysis, Condensation and Densification, *J. Non-Cryst. Solids*, 1984, **63**, 45–59.

23 A. J. Sprockel, M. A. Khan, M. de Ruiter, M. T. Alting, K. A. Macmillan and M. F. Haase, Fabrication of Bijels with Sub-Micron Domains *via* a Single-Channel Flow Device, *Colloids Surf., A*, 2023, **666**, 131306, DOI: 10.1016/j.colsurfa.2023.131306.

24 M. de Ruiter, M. T. Alting, H. Siegel and M. F. Haase, Dual Access to the Fluid Networks of Colloid-Stabilized Bicontinuous Emulsions through Uninterrupted Connections, *Mater. Horiz.*, 2024, **11**, 4987–4997, DOI: 10.1039/d4mh00495g.

25 K. Watanabe, R. Fujinuma, H. Aizawa, H. Namigata, T. A. J. Welling, K. Suga and D. Nagao, A Practical Process for Effective Thickening of Silica Shells Formed onto Spherical Cores by Considering the Variation in Ionic Strength during Sol-Gel Reaction, *Microporous Mesoporous Mater.*, 2024, **379**, 113274, DOI: 10.1016/J.MICROMESO.2024.113274.

26 M. Kaviani, M. Rezaei, S. M. Alavi and E. Akbari, Biogas Dry Reforming over Nickel-Silica Sandwiched Core–Shell Catalysts with Various Shell Thicknesses, *Fuel*, 2024, **355**, 129533, DOI: 10.1016/J.FUEL.2023.129533.

27 T. J. Rottreau, C. M. A. Parlett, A. F. Lee and R. Evans, Diffusion NMR Characterization of Catalytic Silica Supports: A Tortuous Path, *J. Phys. Chem. C*, 2017, **121**(30), 16250–16256, DOI: 10.1021/ACS.JPCC.7B02929/ASSET/IMAGES/LARGE/JP-2017-02929M_0008.JPEG.

28 M. Delgado, A. Lázaro, J. Mazo and B. Zalba, Review on Phase Change Material Emulsions and Microencapsulated Phase Change Material Slurries: Materials, Heat Transfer Studies and Applications, *Renewable Sustainable Energy Rev.*, 2012, **16**(1), 253–273, DOI: 10.1016/J.RSER.2011.07.152.

29 K. Watanabe, R. Fujinuma, H. Aizawa, H. Namigata, T. A. J. Welling, K. Suga and D. Nagao, A Practical Process for Effective Thickening of Silica Shells Formed onto Spherical Cores by Considering the Variation in Ionic Strength during Sol-Gel Reaction, *Microporous Mesoporous Mater.*, 2024, **379**, 113274, DOI: 10.1016/J.MICROMESO.2024.113274.

30 F. Jiao and H. Frei, Nanostructured Cobalt and Manganese Oxide Clusters as Efficient Water Oxidation Catalysts, *Energy Environ. Sci.*, 2010, **3**(8), 1018–1027, DOI: 10.1039/C002074E.

31 J. Govan and Y. K. Gun'ko, Recent Advances in the Application of Magnetic Nanoparticles as a Support for Homogeneous Catalysts, *Nanomaterials*, 2014, **4**, 222–241, DOI: 10.3390/NANO4020222.

32 V. Pellas, J. Blanchard, C. Guibert, J. M. Krafft, A. Miche, M. Salmain and S. Boujday, Gold Nanorod Coating with Silica Shells Having Controlled Thickness and Oriented Porosity: Tailoring the Shells for Biosensing, *ACS Appl. Nano Mater.*, 2021, **4**(9), 9842–9854, DOI: 10.1021/ACSANM.1C02297/ASSET/IMAGES/LARGE/AN1C02297_0006.JPEG.

33 C. Li, Y. Li, Y. Ling, Y. Lai, C. Wu and Y. Zhao, Exploration of the Growth Process of Ultrathin Silica Shells on the Surface of Gold Nanorods by the Localized Surface Plasmon Resonance, *Nanotechnology*, 2014, **25**(4), 045704, DOI: 10.1088/0957-4484/25/4/045704.

34 K. Watanabe, T. A. J. Welling, S. Sadighikia, H. Ishii, A. Imhof, M. A. van Huis, A. van Blaaderen and D. Nagao, Compartmentalization of Gold Nanoparticle Clusters in Hollow Silica Spheres and Their Assembly Induced by an External Electric Field, *J. Colloid Interface Sci.*, 2020, **566**, 202–210, DOI: 10.1016/J.JCIS.2020.01.094.

35 A. Tittl, H. Giessen and N. Liu, Plasmonic Gas and Chemical Sensing, *Nanophotonics*, 2014, **3**(3), 157–180, DOI: 10.1515/NANOPH-2014-0002/ASSET/GRAPHIC/NANOPH-2014-0002_FIG11.JPG.

36 J. Van Wijk, J. W. O. Salari, N. Zaquen, J. Meuldijk and B. Klumperman, Poly(Methyl Methacrylate)–Silica Microcapsules Synthesized by Templating Pickering Emulsion Droplets, *J. Mater. Chem. B*, 2013, **1**(18), 2394–2406, DOI: 10.1039/C3TB20175A.

37 A. M. Bago Rodriguez and B. P. Binks, Capsules from Pickering Emulsion Templates, *Curr. Opin. Colloid Interface Sci.*, 2019, **44**, 107–129, DOI: 10.1016/j.cocis.2019.09.006.

38 Z. Cao, L. Dong, L. Li, Y. Shang, D. Qi, Q. Lv, G. Shan, U. Ziener and K. Landfester, Preparation of Mesoporous Submicrometer Silica Capsules *via* an Interfacial Sol–Gel Process in Inverse Miniemulsion, *Langmuir*, 2012, **28**(17), 7023–7032, DOI: 10.1021/LA300531B/SUPPL_FILE/LA300531B_SI_001.PDF.

39 K. Bean, C. F. Black, N. Govan, P. Reynolds and M. R. Sambrook, Preparation of Aqueous Core/Silica Shell Microcapsules, *J. Colloid Interface Sci.*, 2012, **366**(1), 16–22, DOI: 10.1016/J.JCIS.2011.09.054.

40 H. Wang, X. Zhu, L. Tsarkova, A. Pich and M. Möller, All-Silica Colloidosomes with a Particle-Bilayer Shell, *ACS Nano*, 2011, **5**(5), 3937–3942, DOI: 10.1021/NN200436S/ASSET/IMAGES/LARGE/NN-2011-00436S_0007.JPEG.

41 H. Wu, X. Du, X. Meng, D. Qiu and Y. Qiao, A Three-Tiered Colloidosomal Microreactor for Continuous Flow Catalysis, *Nat. Commun.*, 2021, **12**(1), 6113, DOI: 10.1038/S41467-021-26381-X.

42 H. Gustafsson and K. Holmberg, Emulsion-Based Synthesis of Porous Silica, *Adv. Colloid Interface Sci.*, 2017, **247**, 426–434, DOI: 10.1016/J.CIS.2017.03.002.

43 K. Schumacher, M. Grün and K. K. Unger, Novel Synthesis of Spherical MCM-48, *Microporous Mesoporous Mater.*, 1999, **27**(2–3), 201–206, DOI: 10.1016/S1387-1811(98)00254-6.

44 Q. Huo, J. Feng, F. Schüth and G. D. Stucky., Preparation of Hard Mesoporous Silica Spheres, *Chem. Mater.*, 1997, **9**(1), 14–17, DOI: 10.1021/CM960464P.

45 S. Schacht, Q. Huo, I. G. Voigt-Martin, G. D. Stucky and F. Schüth, Oil-Water Interface Templating of Mesoporous

Macroscale Structures, *Science*, 1996, **273**(5276), 768–771, DOI: 10.1126/SCIENCE.273.5276.768.

46 N. Andersson, B. Kronberg, R. Corkery and P. Alberius, Combined Emulsion and Solvent Evaporation (ESE) Synthesis Route to Well-Ordered Mesoporous Materials, *Langmuir*, 2007, **23**(3), 1459–1464, DOI: 10.1021/LA0622267/ASSET/IMAGES/LARGE/LA0622267F00007.JPEG.

47 A. Venkateswara Rao and S. D. Bhagat, Synthesis and Physical Properties of TEOS-Based Silica Aerogels Prepared by Two Step (Acid–Base) Sol–Gel Process, *Solid State Sci.*, 2004, **6**(9), 945–95210.1016/J.SOLIDSTATESCIENCES.2004.04.010.

48 P. B. Sarawade, J. K. Kim, H. K. Kim and H. T. Kim, High Specific Surface Area TEOS-Based Aerogels with Large Pore Volume Prepared at an Ambient Pressure, *Appl. Surf. Sci.*, 2007, **254**(2), 574–579, DOI: 10.1016/J.APSUSC.2007.06.063.

49 R. Aelion, A. Loebel and F. Eirich, The Hydrolysis and Polycondensation of Tetra Alkoxysilanes, *Recl. Trav. Chim. Pays-Bas*, 1950, **69**(1), 61–75, DOI: 10.1002/recl.19500690109.

50 S. Hæreid, M. A. Einarsrud and G. W. Scherer, Mechanical Strengthening of TMOS-Based Alcogels by Aging in Silane Solutions, *J. Sol-Gel Sci. Technol.*, 1994, **3**(3), 199–204, DOI: 10.1007/BF00486558.

51 J. J. van Beek, D. Seykens and J. B. H. Jansen, ^{29}Si NMR Monitoring and Kinetic Modelling of an Acid-Catalyzed TMOS Sol–Gel System with Molar H_2O/Si = 8, *J. Non-Cryst. Solids*, 1992, **146**, 111–120, DOI: 10.1016/S0022-3093(05)80482-X.

52 M. P. J. Peeters, T. N. M. Bernards and M. J. Van Bommel, ^{17}O-NMR of Sol–Gel Processes of TEOS and TMOS, *J. Sol-Gel Sci. Technol.*, 1998, **13**(1–3), 71–74, DOI: 10.1023/a:1008699104854.

53 J. J. van Beek, D. Seykens and J. B. H. Jansen, ^{29}Si NMR Monitoring and Kinetic Modelling of an Acid-Catalyzed TMOS Sol–Gel System with Molar H_2O/Si = 8, *J. Non-Cryst. Solids*, 1992, **146**(C), 111–120, DOI: 10.1016/S0022-3093(05)80482-X.

54 I. Hasegawa and S. Sakka, Influence of the Type of Alkyl Group on Hydrolysis and Polycondensation of Tetraalkoxysilane, *J. Non-Cryst. Solids*, 1988, **100**(1–3), 201–205, DOI: 10.1016/0022-3093(88)90017-8.

55 F. Fait, S. Wagner, J. C. Steinbach, A. Kandelbauer and H. A. Mayer, Tailoring the Morphology of Monodisperse Mesoporous Silica Particles Using Different Alkoxysilanes as Silica Precursors, *Int. J. Mol. Sci.*, 2023, **24**(14), 11729, DOI: 10.3390/ijms241411729.

56 Z. Zhang, K. C. Tam, X. Wang and G. Sèbe, Inverse Pickering Emulsions Stabilized by Cinnamate Modified Cellulose Nanocrystals as Templates to Prepare Silica Colloidosomes, *ACS Sustainable Chem. Eng.*, 2018, **6**(2), 2583–2590, DOI: 10.1021/ACSSUSCHEMENG.7B04061/ASSET/IMAGES/LARGE/SC-2017-040612_0008.JPEG.

57 H. Jiang, H. Liangzhi, Y. Li, T. Ngai, H. Jiang, T. Ngai, L. Z. Hong and Y. X. Li, All-Silica Submicrometer Colloidosomes for Cargo Protection and Tunable Release, *Angew. Chem., Int. Ed.*, 2018, **57**(36), 11662–11666, DOI: 10.1002/ANIE.201805968.

58 Y. Zhao, Y. Li, D. E. Demco, X. Zhu and M. Möller, Microencapsulation of Hydrophobic Liquids in Closed All-Silica Colloidosomes, *Langmuir*, 2014, **30**(15), 4253–4261, DOI: 10.1021/LA500311Y/ASSET/IMAGES/LARGE/LA-2014-00311Y_0008.JPEG.

59 H. Wang, X. Zhu, L. Tsarkova, A. Pich and M. Möller, All-Silica Colloidosomes with a Particle-Bilayer Shell, *ACS Nano*, 2011, **5**(5), 3937–3942, DOI: 10.1021/NN200436S/ASSET/IMAGES/LARGE/NN-2011-00436S_0007.JPEG.

60 T. Narayanan, M. Sztucki, P. Van Vaerenbergh, J. Léonardon, J. Gorini, L. Claustre, F. Sever, J. Morse and P. Boesecke, A Multipurpose Instrument for Time-Resolved Ultra-Small-Angle and Coherent X-Ray Scattering, *J. Appl. Crystallogr.*, 2018, **51**(6), 1511–1524, DOI: 10.1107/S1600576718012748.

61 M. Sztucki, SAXSutilities: A Graphical User Interface for Processing and Analysis of Small-Angle X-Ray Scattering Data, *Zenodo*, 2021, DOI: 10.5281/ZENODO.5825707.

62 K. S. W. Sing, D. H. Everett, R. A. W. Haul, L. Moscou, R. A. Pierotti, J. Rouquérol and T. Siemieniewska, Reporting Physisorption Data for Gas/Solid Systems with Special Reference to the Determination of Surface Area and Porosity, *Pure Appl. Chem.*, 1985, **57**(4), 603–619, DOI: 10.1351/pac198557040603.

63 M. Thommes, K. Kaneko, A. V. Neimark, J. P. Olivier, F. Rodriguez-Reinoso, J. Rouquerol and K. S. W. Sing, Physisorption of Gases, with Special Reference to the Evaluation of Surface Area and Pore Size Distribution (IUPAC Technical Report), *Pure Appl. Chem.*, 2015, **87**, 1051–1069, DOI: 10.1515/pac-2014-1117.

64 M. F. Haase, K. J. Stebe and D. Lee, Continuous Fabrication of Hierarchical and Asymmetric Bijel Microparticles, Fibers, and Membranes by Solvent Transfer-Induced Phase Separation (STRIPS), *Adv. Mater.*, 2015, **27**(44), 7065–7071, DOI: 10.1002/adma.201503509.

65 M. A. Khan, A. J. Sprockel, K. A. Macmillan, M. T. Alting, S. P. Kharal, S. Boakye-Ansah and M. F. Haase, Nanostructured, Fluid Bicontinuous Gels for Continuous Flow Liquid–Liquid Extraction, *Adv. Mater.*, 2022, 2109547, DOI: 10.1002/adma.202109547.

66 A. A. Issa and A. S. Luyt, Kinetics of Alkoxysilanes and Organoalkoxysilanes Polymerization: A Review, *Polymers*, 2019, **11**, 1–41, DOI: 10.3390/polym11030537.

67 G. De, B. Karmakar and D. Ganguli, Hydrolysis–Condensation Reactions of TEOS in the Presence of Acetic Acid Leading to the Generation of Glass-like Silica Microspheres in Solution at Room Temperature, *J. Mater. Chem.*, 2000, **10**(10), 2289–2293, DOI: 10.1039/b003221m.

68 A. Ray, S. Das and N. Chattopadhyay, Aggregation of Nile Red in Water: Prevention through Encapsulation in β-Cyclodextrin, *ACS Omega*, 2019, **4**, 15–24, DOI: 10.1021/acsomega.8b02503.

69 D. Pontoni, T. Narayanan and A. R. Rennie, Time-Resolved SAXS Study of Nucleation and Growth of Silica Colloids, *Langmuir*, 2002, **18**(1), 56–59, DOI: 10.1021/la015503c.

70 T. Narayanan, Recent Advances in Synchrotron Scattering Methods for Probing the Structure and Dynamics of

Colloids, *Adv. Colloid Interface Sci.*, 2024, **325**, 103114, DOI: **10.1016/j.cis.2024.103114**.

71 L. Wei, S. Yan, H. Wang and H. Yang, Fabrication of Multi-Compartmentalized Mesoporous Silica Microspheres through a Pickering Droplet Strategy for Enhanced CO_2 Capture and Catalysis, *NPG Asia Mater.*, 2018, **10**(9), 899–911, DOI: **10.1038/s41427-018-0083-9**.

72 H. J. Castelijns, H. P. Huinink, L. Pel and P. L. J. Zitha, The Wffect of PH on Coupled Mass Transfer and Sol–Gel Reaction in a Two-Phase System, *J. Phys. Chem. B*, 2007, **111**(43), 12383–12388, DOI: **10.1021/JP073234E**.

73 D. Lee, K. J. Stefe, G. Di Vitantonio and T. Wang, *Robust Bijels for Interfacial Catalysis and Interphase Separations*, US2021.0220791, 2019.

74 L. Y. Yang, H. Z. Li, J. Liu, Z. Q. Sun, S. S. Tang and M. Lei, Dual Yolk–Shell Structure of Carbon and Silica-Coated Silicon for High-Performance Lithium-Ion Batteries, *Sci. Rep.*, 2015, **5**(1), 1–9, DOI: **10.1038/SREP10908;TECHMETA=120,128,145;SUBJMETA=161,354,357,638,639,925;'KWRD=ELECTROCHEMISTRY,NANOPARTICLES**.

75 N. Liu, Z. Lu, J. Zhao, M. T. Mcdowell, H. W. Lee, W. Zhao and Y. Cui, A Pomegranate-Inspired Nanoscale Design for Large-Volume-Change Lithium Battery Anodes, *Nat. Nanotechnol.*, 2014, **9**(3), 187–192, DOI: **10.1038/nnano.2014.6**.

76 N. Liu, H. Wu, M. T. McDowell, Y. Yao, C. Wang and Y. Cui, A Yolk-Shell Design for Stabilized and Scalable Li-Ion Battery Alloy Anodes, *Nano Lett.*, 2012, **12**(6), 3315–3321, DOI: **10.1021/NL3014814/SUPPL_FILE/NL3014814_SI_002.AVI**.

77 T. A. Saleh and V. K. Gupta, An Overview of Membrane Science and Technology, *Nanomaterial and Polymer Membranes*, 2016, pp. 1–23, DOI: **10.1016/B978-0-12-804703-3.00001-2**.